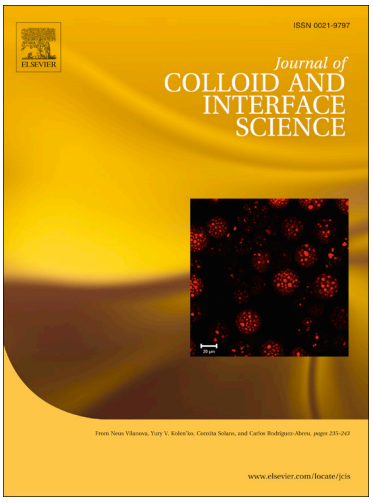

Highly microporous carbon with nitrogen-doping derived from natural biowaste for high-performance flexible solid-state supercapacitor

Fangyan Liu, Yuyu Gao, Haichao Huang, Cheng Yan, Xiang Chu, Zhong Xu, Zixing Wang, Haitao Zhang, Xingbiao Xiao, Weiqing Yang

PII: S0021-9797(19)30419-9
DOI: https://doi.org/10.1016/j.jcis.2019.04.005
Reference: YJCIS 24834

To appear in: *Journal of Colloid and Interface Science*

Received Date: 9 January 2019
Revised Date: 31 March 2019
Accepted Date: 2 April 2019

Please cite this article as: F. Liu, Y. Gao, H. Huang, C. Yan, X. Chu, Z. Xu, Z. Wang, H. Zhang, X. Xiao, W. Yang, Highly microporous carbon with nitrogen-doping derived from natural biowaste for high-performance flexible solid-state supercapacitor, *Journal of Colloid and Interface Science* (2019), doi: https://doi.org/10.1016/j.jcis.2019.04.005

Highly microporous carbon with nitrogen-doping derived from natural biowaste for high-performance flexible solid-state supercapacitor

Fangyan Liu, Yuyu Gao, Haichao Huang, Cheng Yan, Xiang Chu, Zhong Xu, Zixing Wang, Haitao Zhang, Xingbiao Xiao, Weiqing Yang*

State Key Laboratory of Traction Power; Key Laboratory of Advanced Technologies of Materials (Ministry of Education); School of Materials Science and Engineering, Southwest Jiaotong University, Chengdu 610031, China

Fangyan Liu (Dr.) E-mail: liufangyan19881024@126.com.

Yuyu Gao E-mail: lingdantiancai@my.swjtu.edu.cn

Haichao Huang E-mail: huanghaichao@my.swjtu.edu.cn

Cheng Yan E-mail: yancswjtu26@163.com

Xiang Chu E-mail: mrchu@my.swjtu.edu.cn.

Zhong Xu E-mail: zhongxu@my.swjtu.edu.cn

Zixing Wang E-mail: wangzixing817@126.com.

Haitao Zhang (Dr.) E-mail: haitaozhang@swjtu.edu.cn.

Xingbiao Xiao E-mail: 13540791500@163.com

Weiqing Yang (Pro. Dr., corresponding author)

* Corresponding author. Phone:028-87600415; E-mail: wqyang@swjtu.edu.cn

Key Laboratory of Advanced Technologies of Materials (Ministry of Education), School of Materials Science and Engineering, Southwest Jiaotong University, No. 111, North 1st Section of Second Ring Road, Jinniu District, Chengdu 610031, China

Highly microporous carbon with nitrogen-doping derived from natural biowaste for high-performance flexible solid-state supercapacitor

Fangyan Liu, Yuyu Gao, Haichao Huang, Cheng Yan, Xiang Chu, Zhong Xu, Zixing Wang, Haitao Zhang, Xingbiao Xiao, Weiqing Yang†

State Key Laboratory of Traction Power; Key Laboratory of Advanced Technologies of Materials (Ministry of Education); School of Materials Science and Engineering, Southwest Jiaotong University, Chengdu 610031, China

*Corresponding author. E-mail: wqyang@swjtu.edu.cn

Key Laboratory of Advanced Technologies of Materials (Ministry of Education), School of Materials Science and Engineering, Southwest Jiaotong University, No. 111, North 1st Section of Second Ring Road, Jinniu District, Chengdu 610031, China

Abstract

Highly microporous carbon material with nitrogen doping has been synthesized via a facile one-step approach by employing natural biowaste miscellaneous wood fibers as precursor and melamine as nitrogen source respectively. The added melamine not only results in the incorporation of some nitrogen into the carbon framework but also increases the specific surface area of carbon material. Such resultant N-doped microporous carbon possesses the functionalized nitrogen doping (1.75 at. %), a large specific surface area (~ 1807 m^2 g^{-1}), and abundant highly interconnected micropores. Benefiting from the synergistic effect of high specific surface area, well-developed pore size distribution and functionalized groups, this carbon material delivers a high specific capacitance of 345 F g^{-1} at 0.5 A g^{-1}, an excellent capacitance retention with 270 F g^{-1} at up to 30 A g^{-1}, and a remarkable cycle ability with 91.3% retention after 10000 cycles at 5.0 A g^{-1}. Based on it, the as-developed flexible symmetric solid-state supercapacitor delivers a high energy density of 7.92 W h kg^{-1} at the power density of 250 W kg^{-1}. Evidently, this work provides a facile and cost-effective one-step route for functionalized natural biowaste-based carbon materials and further opens up a way for highly value-added recycling of biowaste-like materials.

Key words: biowaste; hydrochar; nitrogen-doping; microporous structure; flexible solid-state supercapacitor

1. Introduction

Supercapacitors have captured global attention as the powerful energy storage devices because of their unique properties that are presently unattainable in lithium-ion batteries, including the superior power density, long lifespan, rapid charge/discharge rate and wide operational temperature range [1-3]. Unfortunately, this kind of storage devices still suffer from the low energy density to date, seriously hampering their further utilization for the increasing demands such as portable consumer electronic devices, electric vehicles, and uninterruptable power supplies. The intrinsic performance of supercapacitor is mainly ascribed to the electrode materials. Typically, the carbon-based materials are universally recognized as the ideal candidates for supercapacitors and have been widely investigated owing to their advantages of stable physico-chemical properties, conductivity, production cost, and so on [4-6]. Compared with carbon materials derived from the non-renewable and unsustainable fossil energy including petroleum pitch, coke and coal, carbon materials coming from natural biomass would be more significant, attractive and worthwhile owing to the cheap cost, renewability, and easy availability [6].

For the biomass-derived carbon materials, their performances are mainly determined by three important factors, namely, the functionalized surface, specific surface area (SSA), and pore size distribution (PSD) [7-10]. Firstly, the surface functionalization with heteroatom-doped especially the representative nitrogen element can provide extra faradaic pseudocapacitance by generating active sites and improve the wettability via changing the electron distribution of carbon materials [8]. Secondly, the large SSA can provide enough accommodation for charge and ion storage and make sure the sufficient

electrolyte/electrode interface to form double electric layers, which is very important for achieving superior performance [7]. The last but not the least, the pore size is distributed reasonably and the micropore size should be smaller than the size of solvated ion but slightly larger than the size of de-solvated ion, since ion solvation shell becomes highly distorted when ion is squeezed through the pore which makes the ion center closer to the electrode surface, resulting in the enhanced capacitance [11]. Currently, it is widely recognized that micropores coexisting with plentiful mesopores in carbon materials is necessary for quick ion diffusion, excellent rate capability and improved power storage property of supercapacitors. However, Gleb Yushin *et al* have proved that mesopores are not indispensable for fast ion transportation and it is possible to realize rapid ion diffusion in micropores attributed to their straight shapes without bottlenecks [12, 13]. Therefore, the biomass-based microporous carbon materials featured with large specific surface area, highly-developed microporous structure and functional incorporation of nitrogen are indispensable to develop for advanced supercapacitors [14].

Besides, the choice of precursor is very important for the carbon material performance. Hydrochar, the highly functionalized carbon materials developed in recent years, can be easily synthesized by the hydrothermal carbonization (HTC) of natural biomass under very mild and green processing condition (autogeneous pressure, < 250 ºC) [15-17]. They generally feature with controlled morphology, uniform structural and chemical properties as well as rich polar functional groups (–OH, –COOH, and –C–O) [18-20]. Importantly, it has shown promising application in energy storage such as supercapacitors, since the hydrochar-derived porous carbons have been proved to possess the better electrochemical

performance than that of carbon materials directly from the crude biomass [21]. In addition, a higher yield of porous carbon could be achieved from hydrochar than pure natural biomass, resulting in the less use of chemical activating agent [21]. However, its intrinsic properties such as no open porosity, low electrical conductivity, and monotonic elements become impediments to application and are need further modified for enhanced-performance supercapacitors. According to the previous reports, converting hydrochar into N-doped microporous carbon usually suffers from two-step process such as heteroatom-doping followed by activation [22]. This two-step technique usually involves the complex, time-consuming and tedious process which seriously hampers their scalable synthesis and applications. Alternatively, the one-step method including N-contained hydrochar with activation or template [23, 24] or adding nitrogenous reagent to the hydrochar/activating agent mixture [25-27] can effectively overcome these disadvantages aforementioned in the two-step process. For the one-step methods, the former is impracticable for the hydrochar without high nitrogen content, whereas the latter would be more attractive, significant and worthy of choice due to its facile, convenient and effective process to co-realize the microporous structure and incorporation of nitrogen into carbon skeleton.

Since biomass-derived hydrochars are demonstrated as an ponderable precursor for high-performance electrode materials, a great variety of natural biomass including hemicellulose [28], potato starch [13, 25], sewage sludge [29] and sawdust [13, 25, 30] have been employed as hydrochar precursors for high-performance porous carbons. As another natural biowaste with huge annual output but being neglected, miscellaneous wood

fibers mainly come from the logging residue in forest region and the marginal waste produced during the wood processing. To the best of our knowledge, the miscellaneous wood fibers-based hydrochar has seldom been applied for the production of N-doped microporous carbon as electrode material for energy storage so far. In this study, we prepare the N-doped microporous carbons with superior electrochemical performance by a facile, effective and sustainable one-step approach which gathers the activation, carbonization, and heteroatom doping process. It employs miscellaneous wood fibers as sustainable precursor, the potassium hydroxide as activating agent and melamine as nitrogen source. The formation of the N-doped microporous carbon is proposed and the morphology, structural, and chemical characteristics have been systematically studied. The as-prepared N-doped microporous carbon exhibits narrow pore size distribution (PSD) mainly focusing on the interconnected micropores, high specific surface area as well as some N-containing functional groups, which is favorable for the enhancement of electrochemical performance. Therefore, the N-doped microporous carbon material delivers a high gravimetric capacitance of 345 F g^{-1} at 0.5 A g^{-1}, excellent rate capacity and superior long-term durability in aqueous electrolyte. Moreover, the symmetric flexible solid-state supercapacitor with N-doped microporous carbon as electrodes and PVA/KOH gel as electrolyte not only output a high energy density of 7.92 W h kg^{-1} at the power density of 250 W kg^{-1} but also displays the excellent flexibility and stability with the achievement of different voltage windows.

2. Experimental

2.1 Materials

All chemical reagents are of analytical purity grade and used without further purification. Natural biowaste, miscellaneous wood fibers, 10–80 mesh, were provided by Hengyou Furniture Group Co., Ltd., Daxing'anling, China. Melamine, potassium hydroxide, and hydrochloric acid were purchased from Chengdu Kelon Chemical Reagent Factory.

2.2 Preparation of wood fiber-derived hydrochar

The hydrochar was produced by hydrothermal carbonization (HTC) of miscellaneous wood fibers. Briefly, the 1 g miscellaneous wood fibers were dispersed in 60 mL ultrapure water and then transferred to 100 mL stainless steel autoclave. Then, the reactor was placed in an oven and heated up to 230 ºC for 14 h. The product was collected by filtration and washed several times with ultrapure water and ethanol, and then dried at 105 ºC for 6 h.

2.3 Preparation of hydrochar-based microporous carbon

The dried hydrochar was chemically activated with the help of potassium hydroxide (KOH). The hydrochar was thoroughly grinded and mixed with KOH at a certain weight ratio (KOH/hydrochar = 2, 3, or 4) in an agate mortar. After that, the mixture was placed in a nickel crucible and directly heated in a tubular furnace under N_2 atmosphere with temperature rising from room temperature to 800 ºC with a heating ramp rate of 3 ºC min^{-1} and held for 1 h. After cooled down, the product was treated with 1 mol L^{-1} HCl solution to eliminate the impurities, and then washed with abundant ultrapure water until neutral PH, and finally dried in the 105 °C oven for 6 h.

According to the weight ratio of KOH / hydrochar, the products were labeled as H-MPC-X, where H is the hydrochar, MPC means the microporous carbon and the X is the KOH/hydrochar weight ratio, *i.e.*, 2, 3 or 4.

2.4 Preparation of N-doped MPC

In the preparation process of the N-doped hydrochar-based MPC, the melamine ($C_3H_6N_6$) was selected as nitrogen source. Typically, the hydrochar, KOH, and melamine are thoroughly mixed at a weight ratio of 2: 6: 1 and then pyrolyzed at 800 °C in an agate mortar for 1 h under N_2 atmosphere. The obtained product was washed with 1 mol L^{-1} HCl solution and then with ultrapure water until PH was neutral, and finally dried in the 105 °C oven for 6 h. The obtained product is denoted as H-MPC-N.

2.5 Materials characterizations

Scanning electron microscopy (SEM, JEOL JSM-7001F) equipped with energy dispersive spectroscopy (EDS), transmission electron microscopy (TEM, FEI Tecnai G2 F20) and high-resolution TEM (HRTEM) were employed to characterize the morphology, element distribution, microstructure of the samples. The X-ray diffraction (XRD) patterns of the products were acquired with the aid of PANalytical X'Pert Powder diffractometer. Raman spectroscopy were performed on the Thermo Fisher DXR (Raman) spectrometer with laser excitation at a wavelength of 514 nm. N_2 (77K) adsorption/desorption isotherms and textural properties of the samples were obtained by a Quantachrome 2SI-MP-9 surface area and pore size analyzer. The specific surface areas (SSA) of the samples were evaluated based on the Brunauer-Emmett-Teller (BET) method while their pore size distribution (PSD) was determined by the Non-local Density Functional Theory (NLDFT) method. The

surface chemical information of the samples was detected by X-ray photoelectron spectroscopy (XPS, Thermo Fisher ESCALAB 250Xi).

2.6 Electrochemical measurements

The electrochemical performances of the samples were measured in a three-electrode system. For the preparation of working electrode, the carbon material was mixed with acetylene black (conductive additive) and polytetrafluoroethylene (PTFE, binder) in a weight ratio of 8: 1: 1, then the mixture was thoroughly blended in ethanol and dried at 80 °C for eliminating the ethanol. After that, the mixture was rolled into film with thickness about 80−100 μm and punched into disk-like electrode with diameter of 12 mm. After dried at 110 °C for 8 h, the electrode was pressed onto the nickel foam. In this three-electrode system, the Pt foil (2 cm ×2 cm) was employed as the counter electrode and the Hg/HgO electrode as the reference electrode in 6 mol L^{-1} KOH aqueous electrolyte. The electrochemical performance of H-MPC-N was also measured in two-electrode configuration with PVA/KOH gel electrolyte. For the preparation of PVA/KOH gel electrolyte, 4 g PVA (1799 type) was dissolved in 25 mL ultrapure water under vigorous stirring at 85 °C until the complete dissolution of PVA. Then, 4 g KOH that dissolved 15 mL ultrapure water was added dropwise into the PVA solution with continuous stirring. Finally, the clear PVA/KOH gel with homogeneous viscous appearance was prepared. Two working electrodes were immersed into the PVA/KOH gel electrolyte, and then placed in air for several minutes, and finally assembled in parallel to fabricate a symmetric sandwich-like supercapacitor. To encapsulate the flexible solid-state supercapacitors, the PET films were adopted.

Cyclic voltammetry (CV), galvanostatic charge-discharge (GCD), and the electrochemical impedance spectroscopy (EIS) in the frequency ranging from 100 kHz to 0.01 Hz at the amplitude of 5 mV were performed on a CHI660E electrochemical working station (Shanghai Chenhua Instrument, Inc., China). The cycling durability of the sample was conducted on a LAND cell measurement system. The calculation formulas of specific capacitance (C, F g^{-1}), energy density (E, W h kg^{-1}), and power density (P, W kg^{-1}) are provided in the Supplementary Information.

3. Results and discussion

3.1 Formation of the N-doped microporous carbon

The three-dimensional N-doped microporous carbon was prepared via a facile HTC treatment, followed by one-pot approach combining the activation, carbonization, and heteroatom doping process. The detailed preparation process is exhibited in Figure S1. The miscellaneous wood fibers were firstly under hydrothermal treatment for the totally conversion into hydrochars. Subsequently, the acquired hydrochars mixing with melamine and KOH are heat-treated under N_2 atmosphere. Eventually, the N-doped microporous porous carbon was obtained after thoroughly washed with water and dried in the oven. During the KOH activation process, the hydrochar reacts with KOH that described as 6 KOH + 2 C $\rightarrow$ 2 K + 2 K_2CO_3 + 3 H_2 [31, 32]. There are a series of the intermediate products such as K_2CO_3, CO_2 and K_2O produced in the process of KOH activation. Among them, the K_2CO_3 and CO_2 can be further reduced by carbon to create the pores. At high activation temperature over 700 °C, the metallic potassium originating from the reaction of

K_2CO_3 and K_2O with carbon becomes vapour and easily intercalates into the carbon backbone, therefore giving rise to lots of developed micropores [32]. Meanwhile, the melamine firstly polymerizes to produce a carbon nitride allotrope (*g*-C_3N_4) acting as the 2 D layered template when the mixture was heated to 500 °C [25]. With further increasing the temperature from 500 to 800 °C, the *g*-C_3N_4 undergoes decomposition, generating some reactive nitrogen-containing species ($C_2N_2^+$, $C_3N_2^+$, $C_3N_3^+$, etc.) which react with the semi-carbonized materials [33] and hence realizing the incorporation of nitrogen-containing groups into the carbon framework. In parallel, the KOH activation and melamine jointly promote the formation of N-doped microporous carbon.

3.2 Structural and chemical properties of the carbon materials

The morphology information of the samples was achieved with the aid of scanning electron microscopy (SEM), as presented in Figure 1. The miscellaneous wood fibers consist of numerous single tubular wood cell with high length-diameter ratio (Figure 1a). After HTC, the wood fibers have been converted into hydrochar with irregular morphology including various size carbon spheres, and their original structure have been completely disappeared (Figure 1b). After hydrochar treated with KOH, the product H-MPC-2 presents a porous structure with 3 D substantial interconnected channels (Figure 1c), similarly, the H-MPC-3 also possesses plentiful macropores in the 3 D porous structure but the thinner carbon wall and more sophisticated connected internal transport due to the increased amount of KOH (Figure 1d). The macropores can be served as ion-buffering accommodation space and the complex interconnected channels are beneficial for the fast

shuttle of electrolyte ion. Increasing the KOH/hydrochar ratio to 4, the carbon material mainly consists of collapsed partial sections due to the excessive activation of KOH (Figure 1e). After nitrogen doping, the obtained carbon material shows a different morphology with above activated carbons (Figure 1f), and it not only exhibits the porous structure but also the 2 D carbon sheets featuring with thin layers which could promote the electrolyte ion quickly shuttle in the electrode surface and internal channels [24]. The existence of 2 D sheet-like structure can be also observed in the TEM image of H-MPC-N (Figure 1g). As shown in Figures 1h-i, some circle-like mesopores and abundant worm-like narrow micropores are well developed and randomly distributed in this carbon material. In addition, the high resolution transmission electron microscopy (HRTEM) image demonstrates that this carbon material is composed of dominant amorphous carbon structure accompanied by tiny range-ordered graphitic region since many distorted lattice fringes which could be seen clearly in Figure 1j. The formation of graphene-type layers is conductive to improve the electrical conductivity. The TEM and HRTEM images of the H-MPC-3 are provided in Figure S2, which presents more the block outline with numerous micropores and graphitic region. The results of HRTEM images also imply that KOH activation mainly creates plentiful micropores in carbon materials, which is corroborated by the N_2 adsorption-desorption isotherms and PSD curves displayed in Figures 2a-b.

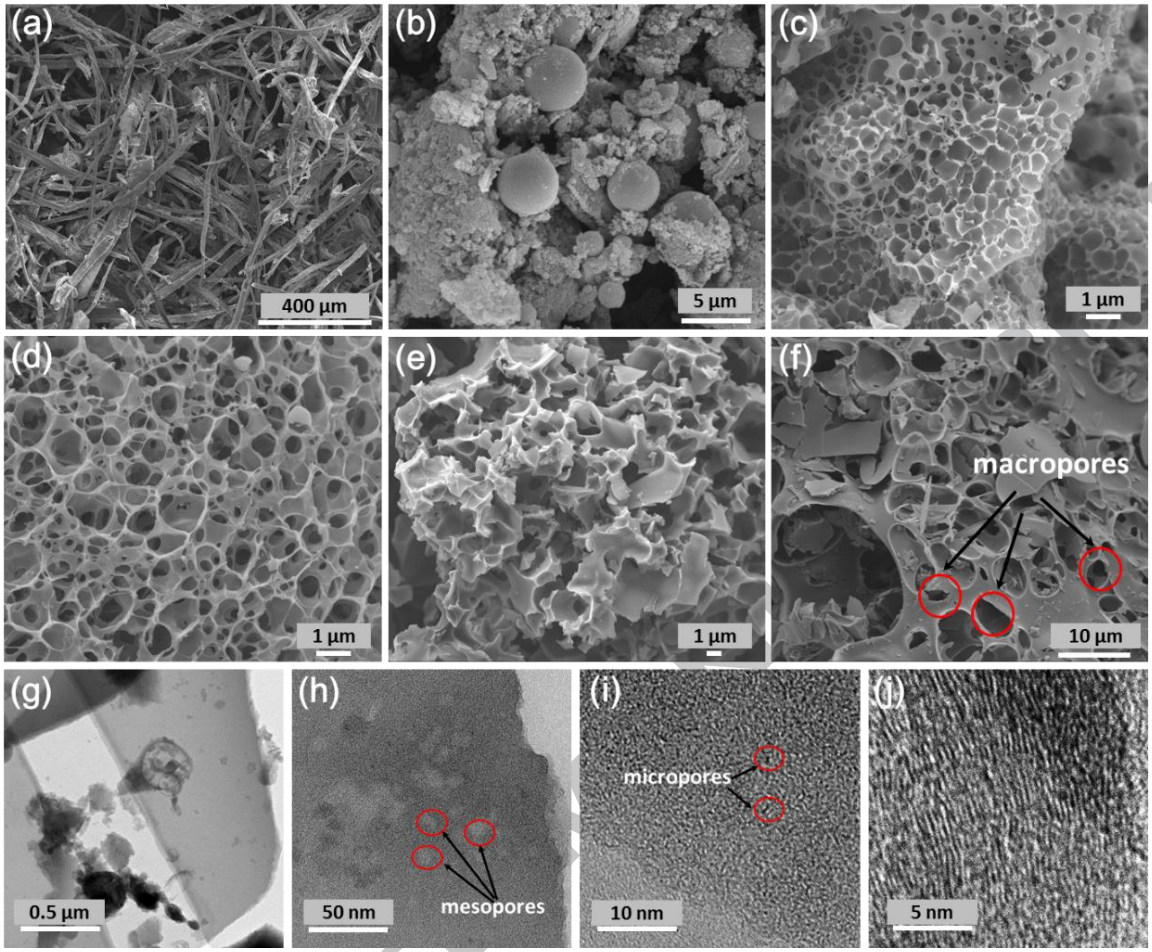

Figure 1. The SEM images of (a) wood fibers, (b) hydrochar, (c) H-MPC-2, (d) H-MPC-3, (e) H-MPC-4 and (f) H-MPC-N; the (g-i) TEM and (j) HRTEM images of H-MPC-N.

Apparently, the H-MPC-3, H-MPC-4 and H-MPC-N display a typical type-I according to the IUPAC classification. A steep increase absorption in the low-pressure region (P/P_0 < 0.2) and no hysteresis between the adsorption and desorption branches are characteristic for microporous materials [13]. As for the H-MPC-2, it shows a type-IV isotherm with a sudden increase when P/P_0 < 0.2 and a H4 hysteresis loop at the middle and high relative pressure (P/P_0 > 0.5), demonstrating its hierarchical porous structure. The SSA is particularly important for many SSA sensitive applications and the total SSA of these carbon materials calculated based on the Brunauer-Emmett-Teller (BET) equation are

ranging from 990.3 to 1807 m^2 g^{-1} (Table 1). Especially, it can be found from Table 1 that the micropore surface areas of H-MPC-3, H-MPC-4 and H-MPC-N are very close to their total SSA, further demonstrating the microporous nature of the three carbon materials. Besides the SSA, the PSD is another crucial parameter influencing the electrochemical performance of carbon-based materials, calculated using the DFT calculations and exhibited in Figure 2b. All carbon samples show narrow PSD that mainly focusing on the narrow micropores (< 1 nm) and super-micropores (1−2 nm) with pore volume from 0.635 to 0.836 cm^3 g^{-1}. Obviously, without the N doping, both SSA and pore volume of these samples increase with the KOH amount increasing. After incorporation of nitrogen, the H-MPC-N shows the highest SSA and largest pore volume, suggesting the addition of melamine is favorable for the enhancement of SSA and pore volume.

The phase structures of the samples were examined by X-ray powder diffraction (XRD). As displayed in Figure 2c, two broad (002) and (100) diffraction peaks are approximately centered at 23.7º and 43º for H-MPC-2, H-MPC-3, and H-MPC-4, respectively, implying the amorphous structure of the three samples. Apparently, the intensity of (002) peak becomes strong with the increment of KOH amount, indicating the enhancement of the non-graphitic structure. After the addition of melamine, the (002) peak shifts toward from 23.7º to lower angle 20.0º and its intensity increases remarkably, suggesting the increased defected structure. The microstructure of samples was also further investigated by Raman spectroscopy. As manifested in Figure 2d, two well-known characteristic D band (defective and disordered carbon) and G band (graphitic carbon) were observed around at 1322 and 1581 cm^{-1}, respectively. It is well known that the intensity ratio of D to G bands (I_D/I_G) for

these carbon materials could reflect the degree of structural disorder. The calculated I_D/I_G ratios of H-MPC-2, H-MPC-3, H-MPC-4, and H-MPC-N are 1.01, 1.06, 1.07, and 1.08, respectively, implying the H-MPC-N possesses larger defects in structure than H-MPC-2, H-MPC-3 and H-MPC-4. Obviously, with enhancement the concentration of KOH and the addition of melamine, the I_D/I_G ratios gradually increase, inferring that deeper activation and decomposition of melamine could promote the growth of defective and disordered section in these carbon materials. The above results prove that the hydrochar-derived carbon materials mainly possess the microporous structure accompanied by amorphous nature with low graphitization degree.

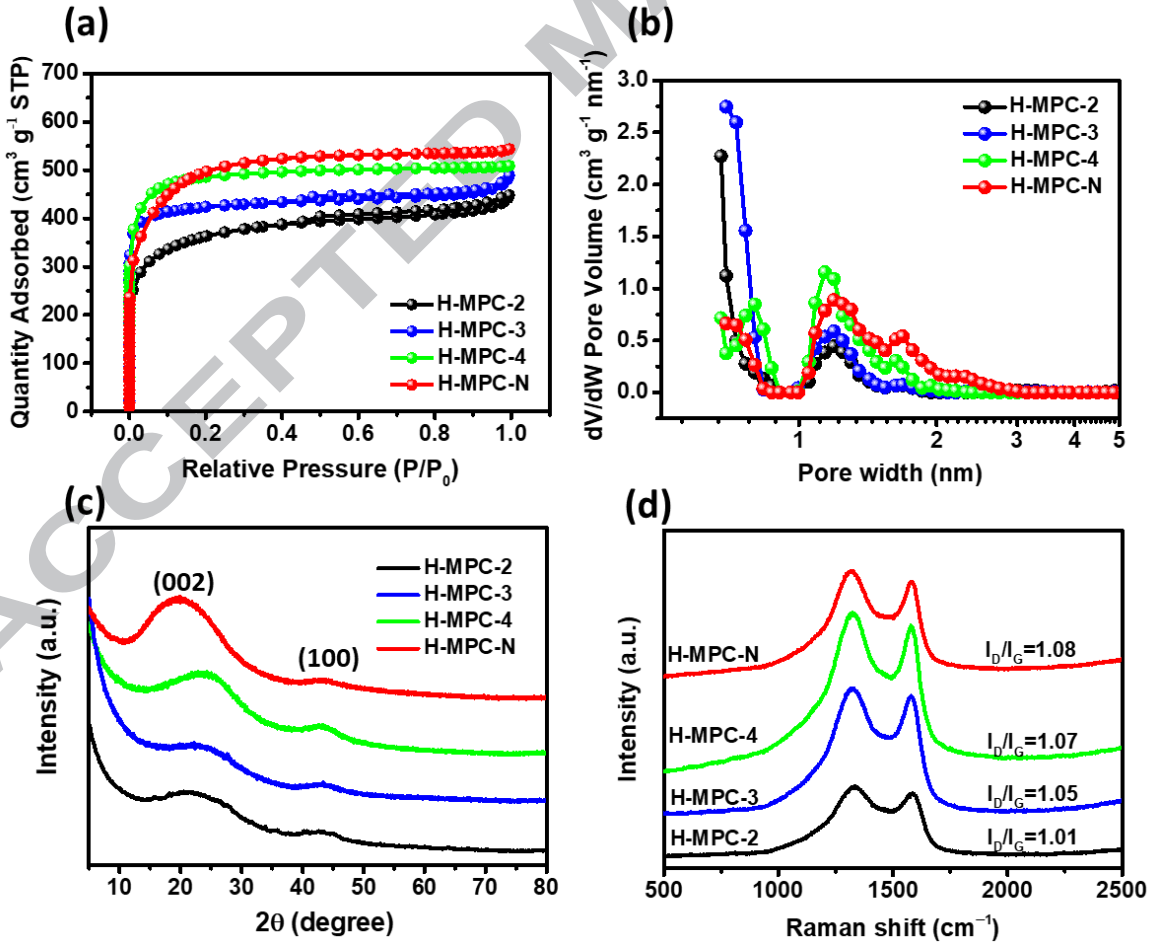

Figure 2. (a) N_2 adsorption-desorption isotherms; (b) pore size distribution curves determined by NLDFT method; (c) XRD patterns and (d) Raman spectra of H-MPC-2, 3, 4 and H-MPC-N.

Table 1. The porosity parameters, surface elemental compositions and electrochemical performances of H-MPC-2, 3, 4 and H-MPC-N.

	N_2 adsorption-desorption					XPS			Three-electrode
	SSA ($m^2\ g^{-1}$)			Pore volume ($cm^3\ g^{-1}$)		Element content (at. %)			system C_g ($F\ g^{-1}$)
Sample	S_{BET}[a]	S_{micro}[b]	S_{ext}[c]	V_{total}[d]	V_{micro}[e]	C	O	N	
H-MPC-2	990.3	859.9	130.4	0.635	0.386	92.55	7.33	0.12	275
H-MPC-3	1485	1428	57	0.736	0.639	91.97	7.92	0.11	300
H-MPC-4	1723	1680	43	0.785	0.743	91.01	8.91	0.08	261.5
H-MPC-N	1807	1743.5	63.5	0.836	0.775	88.75	9.5	1.75	345

[a] Specific surface area (S_{BET}) was calculated with BET method; [b, c] Specific micropore surface area (S_{micro}) and specific external surface area (S_{ext}|) are calculated using t-plot method; [d, e] Total pore volume (V_{total}) was determined at a relative pressure of 0.98 and micropore volume (V_{micro}) was obtained by the t-plot analysis. The C_g values obtained from the discharge curves at the current density of 0.5 $A\ g^{-1}$.

Surface chemical composition characterization of the samples measured by X-ray photoelectron spectroscopy (XPS) is presented in Figure 3a. As listed in Table 1, the increase in the KOH/hydrochar mass ratio promotes the successively increase of the surface oxygen content. This enhancement of surface oxygen content is ascribed to the KOH activation which introduces the oxygen-containing functional groups into these porous carbons [34]. Although the nitrogen element is detected in H-MPC-2, H-MPC-3 and H-MPC-4, their contents are really minor, hence, only the peaks of C 1s and O 1s located around binding energy of 284.7 and 533.2 eV are observed in the full scan spectra of H-MPC-3 (Figure 3a). After 1.75 at. % of nitrogen element incorporated in H-MPC-N, not only C 1s and O 1s peaks but also the N 1s around 401 eV can be detected. The C 1s spectrum of H-MPC-N could be fitted into four different peaks at the binding energies of 284.8, 286, 287 and 288.9 eV, attributing to the C-C/C=C, C-N/C-O, C-O-C and O-C=O configurations, respectively (Figure 3b) [35-37]. For the O 1s, it can be deconvoluted into four peaks located at 530.8, 531.9, 532.7, and 535.3 eV which are pointed to quinone-type oxygen, carbonyl groups (C=O), C-O-C/C-OH, and O=C-OH carboxylic groups or absorbed water, respectively (Figure 3c) [38]. The high-resolution N 1s spectrum in Figure 3d is resolved into four individual peaks, assigning to pyridinic N (N-6) at 398.7 eV, pyrrolic N (N-5) at 399.6 eV, quaternary N (graphitic N, N-Q) at 400.6 eV and oxidized pyridinic N (N-X) at 402.0 eV [34, 38, 39]. The exposed N-5 and N-6 play a paramount role in the pseudocapacitance contribution, since the N-5 serves as electron-donor which can enhance the carbon catalytic activity during the electron-transportation while the N-6 could introduce active sites for pseudocapacitance, and the N-Q facilitates electron transfer

through the carbon matrix [38]. The feasible location of heteroatoms doped into the chemical structure of H-MPC-N is illustrated in Figure 3e. More than that, the elemental mapping images demonstrates that the carbon, oxygen, and nitrogen elements are uniformly distributed in H-MPC-N (Figure 3f). These results definitively prove that the successful conversion of natural biowaste miscellaneous wood fibers into N-doped functionalized carbon.

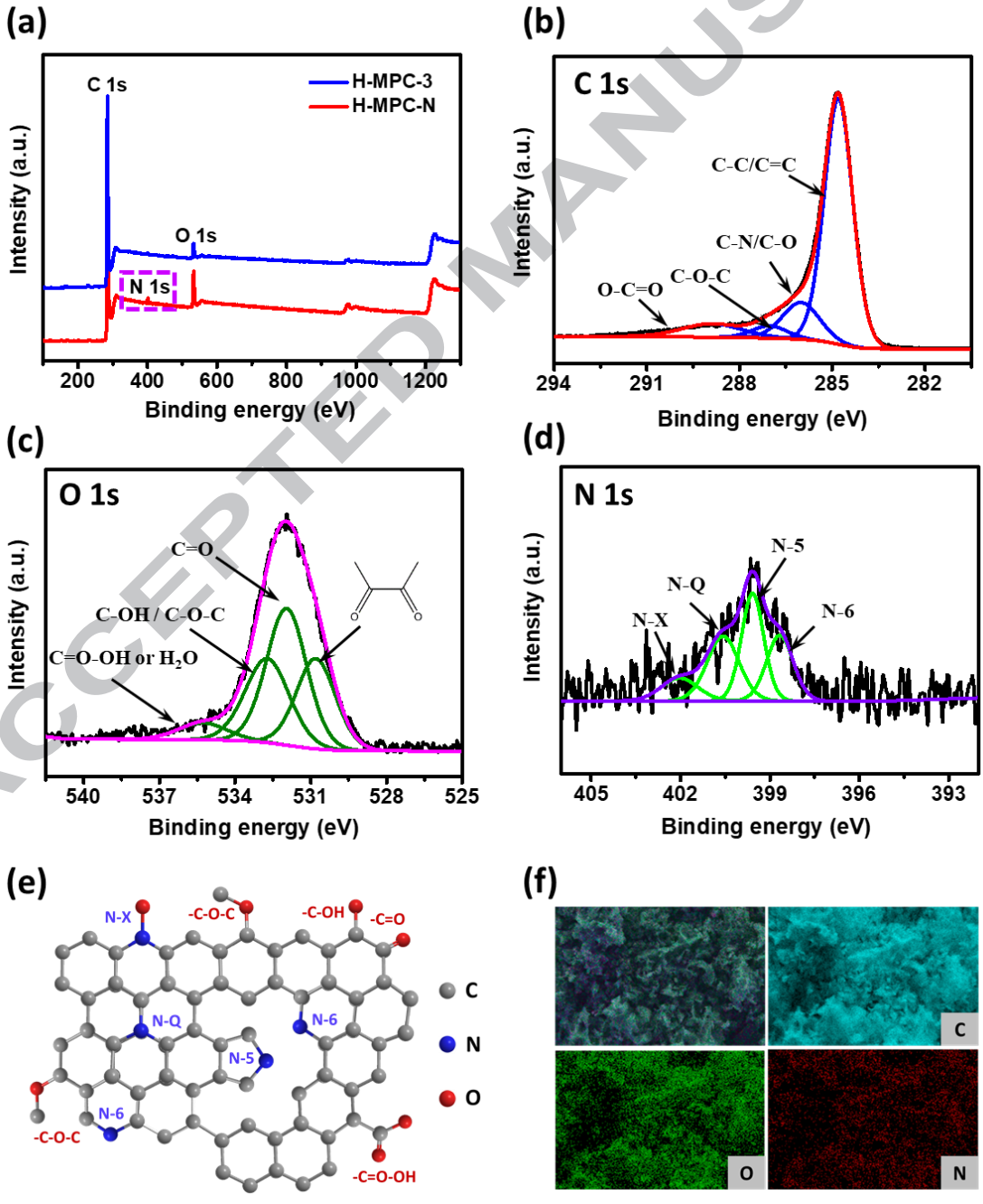

Figure 3. (a) XPS survey spectra of H-MPC-3 and H-MPC-N; the high-resolution XPS spectra of (b) C 1s, (c) O 1s, and (d) N 1s of H-MPC-N; (e) A feasible schematic illustration for the chemical structure of H-MPC-N; and (f) Elemental mapping images of H-MPC-N for carbon, oxygen and nitrogen.

On account of the attractive characteristics such as quintessential microporous structure, high specific surface area and heteroatom doping, the H-MPC-N has high expectation of being a superior electrode material for supercapacitors. The cyclic voltammetry (CV) and galvanostatic charge/discharge (GCD) measurements in a three-electrode configuration with 6.0 M KOH electrolyte are first conducted to investigate the electrochemical performance of these carbon materials. As displayed in Figure 4a, the samples exhibit the rectangle-like CV curves with bumps (caused by redox reactions) at the scan rate of 10 mV s^{-1}, implying the dominated electrical double-layer capacitive behavior accompanied by pseudocapacitance attributed to the functional groups. Compared with H-MPC-2 and H-MPC-4, the H-MPC-3 obviously possesses a larger closed area, indicating the KOH/hydrochar weight ratio of 3 should be an optimal choice which can achieve the better electrochemical performance. Normally, the specific capacitance is directly proportional to SSA of the electrode material [40], however, the H-MPC-3 has no the highest SSA, largest pore volume or maximum content of heteroatom but possesses the largest specific capacitance. Interestingly, this abnormal relationship between the SSA and gravimetric specific capacitance is rather common in the previous paper with different opinions [9, 40-42]. The anomaly in this work should be probably attributed to that: the solvated and bare ion sizes of K^+ are 0.331 nm and 0.133 nm while those of OH^- are 0.300 nm and

0.176 nm [43], and the pore size of H-MPC-2, H-MPC-3 and H-MPC-4 mainly focuses on 0.694, 0.675, and 0.675 (and 0.801) nm, respectively, and those pores were substantially slightly larger than twice the size of solvated K^+ and OH^- ions. The capacitances of these carbon materials is contributed by the compact layers of ions residing on both adjacent pore walls [11]. Compared with other size pores, the pore located at 0.675 nm is easier to achieve high capacitance since ion center is closer to the electrode surface, especially, the pore volume of pore size located at 0.675 nm of H-MPC-3 is much larger than that of H-MPC-2 and H-MPC-4, hence, the H-MPC-3 has the largest capacitance. More than that, the larger SSA of H-MPC-3 is also the main reason for the higher specific capacitance of H-MPC-3 than that of H-MPC-2. Therefore, the good electrochemical performance of H-MPC-3 mainly comes from the synergistic effect of its SSA and PSD. Dramatically, after nitrogen doping, the H-MPC-N owns a much larger closed area than that of these carbon materials without nitrogen doping treatment, suggesting the increased energy storage capability. The reason behind the enhancement of capacitance in H-MPC-N is fairly well understood. Firstly, the doped pyrrolic and pyridinic nitrogens introduce the extra pseudocapacitance to the double layer capacitance since these two kinds of nitrogens with electrochemical activity control electronic structures and the accommodation of K^+ on the electrode surface, and the water around the K^+ near the electrode surface can produce redox reactions between water and electrochemically active functional group, and hence increasing the specific capacitance; the introduced graphitic nitrogen can improve the electronic conductivity of the H-MPC-N, which is beneficial for the electrons transfer in the electrode. Secondly, besides the nitrogen doping, the oxygen-based functional groups

especially the quinone and carbonyl groups can enhance the hydrophilia of carbon materials and possess the electrochemical activity, which is favorable for the electrochemical performance [38]. The last but not the least, the H-MPC-N has the largest SSA, and the surface functional groups can grasp the ions and thus take full advantage of its specific surface area, which can provide more accommodation for charge and ion storage. The GCD profiles of samples at the current density of 0.5 A g^{-1} are shown in Figure 4b. The GCD profiles of H-MPC-2, 3, 4 show a slight deviation from the standard triangular shape suggest their excellent capacitive behaviors accompanied by Faradaic reactions induced by oxygen-containing functionalities. As for H-MPC-N, the deviation of GCD profile increases, attributing to the increased oxygen content and the doped nitrogen element. The H-MPC-N possesses the longest discharging time, inferring the largest specific capacitance, which is consistent with the result of CV curves. The CV and GCD curves of the H-MPC-N still hold a rectangle-like and similar isosceles triangle shapes even at the scan rate of 100 mV s^{-1} and ultrahigh current density of 30 A g^{-1}, indicating the superior rate capability (Figures 4c-d). The specific capacitances of these four samples calculated from the discharging time are shown in Figure 4e. The H-MPC-N enjoys the highest gravimetric specific capacitance of 345 F g^{-1} at 0.5 A g^{-1} and still retains 270 F g^{-1} even at a rather high current density of 30.0 A g^{-1} with 78.2% capacitance retention. What's more, compared with other biomass-derived carbon materials reported previously, the electrochemical performance of H-MPC-N is competitive, as presented in Table S1. The gravimetric capacitances of H-MPC-2, H-MPC-3, and H-MPC-4 at 0.5 A g^{-1} are 275 F g^{-1}, 300 F g^{-1}, and 261.5 F g^{-1}, respectively, with continuing to enhance the current density to

30.0 A g^{-1}, the capacitances are still retained 240 F g^{-1}, 249 F g^{-1}, and 230 F g^{-1}, respectively. Additionally, the cycle life is another significant evaluation index for electrode materials in practical application. After 10000 cycles at 5.0 A g^{-1}, the H-MPC-N still holds a high capacitance retention of 91.3%, confirming the excellent long-term cycling performance (Figure 4f).

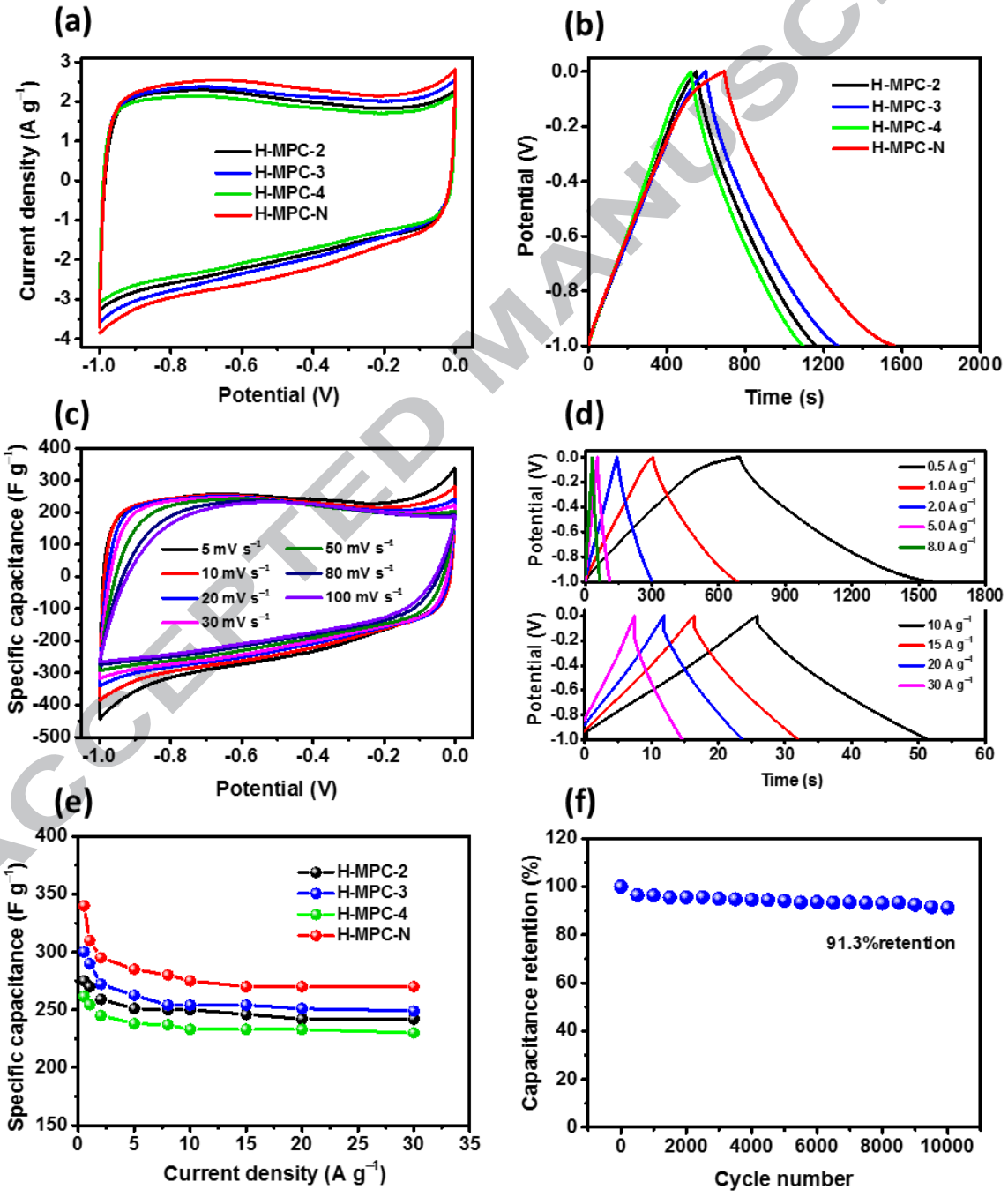

Figure 4. Electrochemical performances of the H-MPC-2, 3, 4 and H-MPC-N measured in 6 M KOH using the three-electrode system. (a) CV curves at 10 mV s^{-1} and (b) GCD profiles at 0.5 A g^{-1} of H-MPC-2, 3, 4 and H-MPC-N; (c) CV curves of H-MPC-N at the scan rates from 5−100 mV s^{-1}; (d) GCD profiles of H-MPC-N at the current densities of 0.5−30 A g^{-1}; (e) Specific capacitances calculated at different current densities; and (f) Cycle stability of H-MPC-N at 5.0 A g^{-1} after 10000 cycles.

In order to examine the practical performance of H-MPC-N, the symmetrical solid-state supercapacitor with flexibility has been fabricated with two identical H-MPC-N-based electrodes in the PVA/KOH gel electrolyte, as illustrated in Figure 5a. The electrochemical performances of flexible solid-state supercapacitor assembled with H-MPC-N were investigated in detail. As presented in Figure 5b, the curves of the symmetrical supercapacitor in the operating voltage window of 0−1.0 V show the rectangle-like shape without apparent distortion, suggesting the quintessential electrical double-layer capacitive performance. Additionally, GCD profiles show the symmetrical charging and discharging curves, further demonstrating the good capacitive behaviour (Figure 5c). For the better understanding of the electrochemical behavior of the flexible solid-state supercapacitor, the electrochemical impedance spectroscopy (EIS) measurement was conducted. As shown in the Figure 5d, the Nyquist plot of the device shows the almost vertical line in the low frequency range, suggesting the approximate ideal capacitive behavior of this device. The Warburg resistance with 45º slope in the middle frequency region indicates the dominant ion diffusion/transport in electrolyte [44]. According to the magnified data in high frequency range (Figure 5d, inset), the equivalent series resistance (ESR, the sum of

intrinsic resistances of electrode materials, the contact resistance of electrode with current collector and ionic resistance of electrolyte) of 0.66 ohm can be obtained by the intercept at the real axis in the high frequency, exhibiting the small internal resistance of the device [45]. It is widely recognized that the semicircle could present the electrochemical reaction impedance of the electrode [46], and the small semicircle observed in the high frequency region implies the small charge transfer resistance (R_{ct}) between electrode and electrolyte. The good electrochemical performance of the H-MPC-N-based flexible device is mainly ascribed to its large effective SSA in the microporous structure, the existed graphite region which is favorable for the ion diffusion/transport and decrease the ion shuttle resistance especially in the large current densities as well as the heteroatom-doping. The as-integrated H-MPC-N-based supercapacitor possesses a high gravimetric specific capacitance of 228 F g^{-1} at 0.5 A g^{-1} calculated based on the one electrode mass, and still outputs 190 F g^{-1} at a very high current density of 20 A g^{-1}, signifying an outstanding rate performance with 83.3% retention (Figure 5e). The flexible symmetric supercapacitor also shows good cycle performance, and 92.2% of the initial capacitance at the current density of 2.0 A g^{-1} after 10000 cycles is retained in the potential window of 0−1.0 V, implying the superior cycle life of the device (Figure 5f).

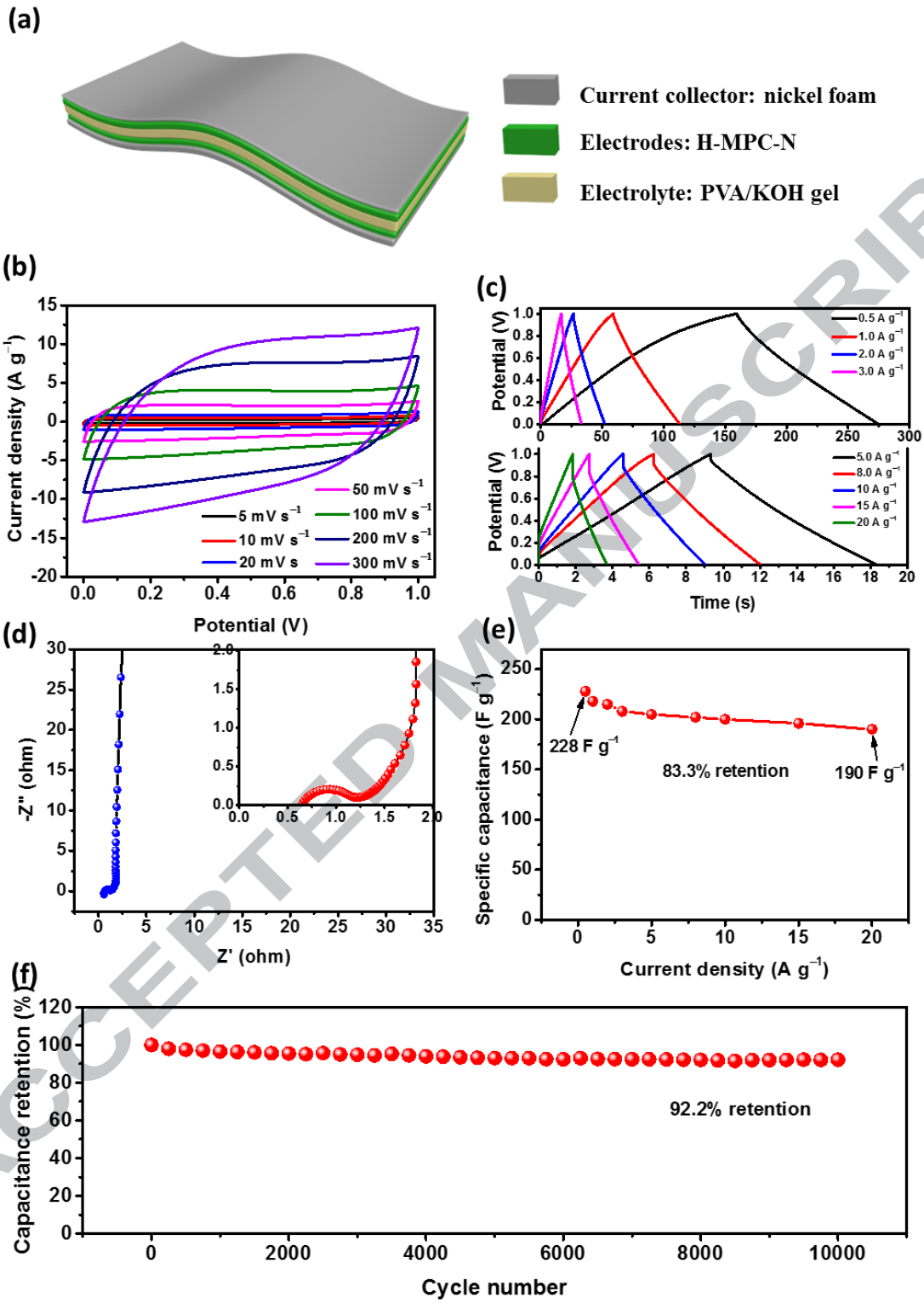

Figure 5. Electrochemical performances of the flexible solid-state supercapacitor assembled with H-MPC-N measured in PVA/KOH gel electrolyte. (a) Schematic diagram of the flexible solid-state supercapacitor; (b) CV curves at various scan rates; (c) GCD

profiles at different current densities; (d) Nyquist plot; (e) Specific capacitances calculated at different current densities; and (f) Cycling performance of the device at 2.0 A g^{-1} after 10000 cycles.

To evaluate the practical prospects of the micro and portable energy storage device with flexibility, the energy density and power density of this device are calculated and the Ragone plot is illustrated in Figure 6a. Obviously, the energy density gradually deteriorates along with the increment of power density. The device outputs the energy densities of 7.92−4.11 W h kg^{-1} at the power densities of 250−7939 W kg^{-1}, which is better than that of some biomass derived carbon-based devices reported previously [28, 47-52]. Equally importantly, the flexibility of device is also investigated by bending the device in 90 and 180º together with the CV measurement at the scan rate of 50 mV s^{-1} and the corresponding results are shown in Figure 6b. It can be seen that there is almost no obvious distortion in the CV curves or reduction in its capacitance, indicating its excellent flexibility and stability. Additionally, the H-MPC-N-based flexible solid-state supercapacitors can be connected in parallel or in series to obtain the augmented discharging time and working potential. At the current density of 1.0 A g^{-1}, the integrated devices in parallel or in series connection output almost twice charge-discharge time, or twice and three voltage windows of a single device (Figure 6c). The stable working potential of the connected devices could make sure their good practical application. As shown in Figure 6d, a green LED lamp with operating voltage of 3 V was lit up by three flexible solid-state supercapacitors connected in series. These abovementioned results show that the H-MPC-N-based flexible solid-state supercapacitors possess the good

electrochemical performance, superior flexibility, and feasibility with different working potential, suggesting the large potential of H-MPC-N-based electrodes in the micro and portable energy storage devices.

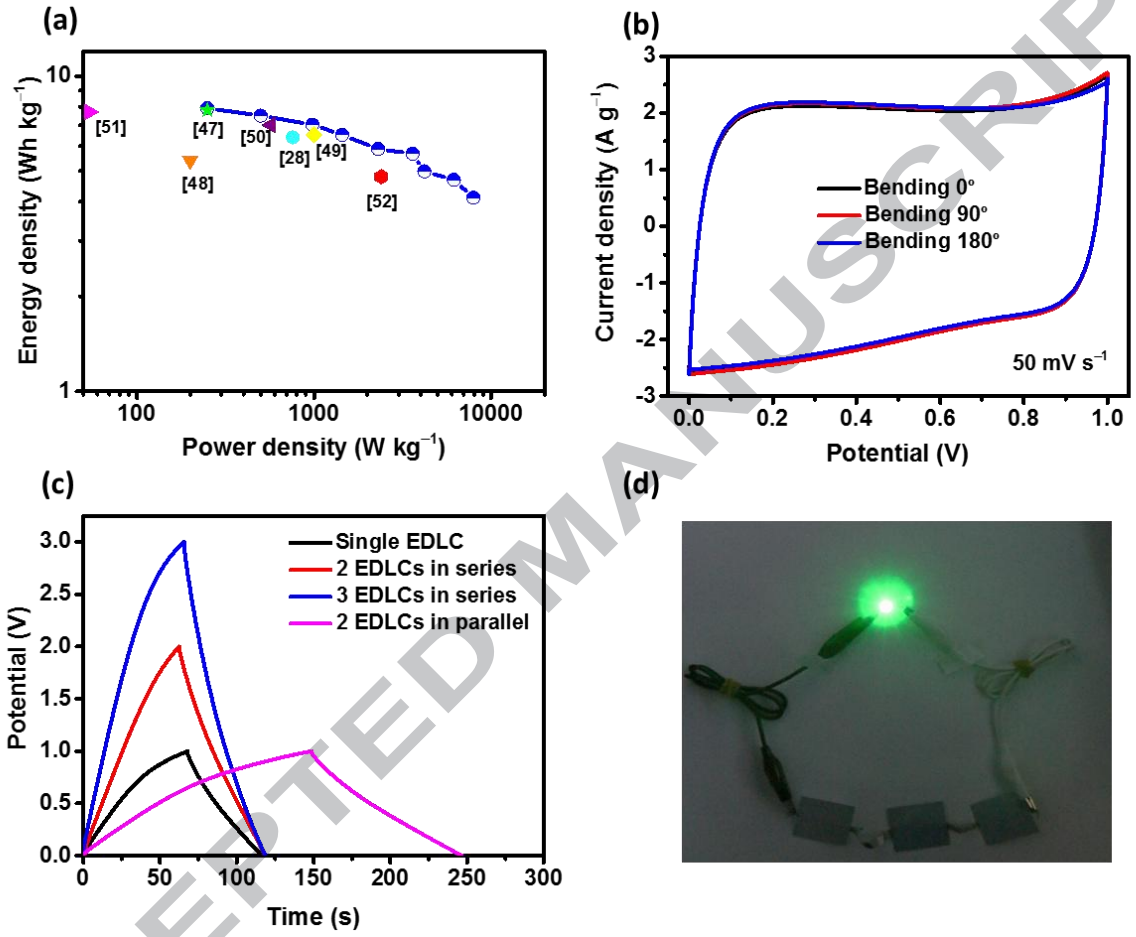

Figure 6. Application performance of the H-MPC-N-based flexible solid-state supercapacitors. (a) Ragone plot; (b) CV curves of the device in bent states; (c) GCD profiles of a single supercapacitor, two supercapacitors connected in parallel and in series, and three supercapacitors in series connection at 1.0 A g^{-1}; and (d) Photographs of a green LED lit up by three flexible solid-state supercapacitors in series connection.

4. Conclusion

In this work, the N-doped microporous carbon material has been successfully prepared from biowaste miscellaneous wood fibers-derived hydrochar by a simple one-step approach combining the activation, carbonization, and heteroatom doping process. This method is facile, effective, and sustainable while the raw material is abundant, almost "zero-cost", and totally green. The developed N-doped microporous carbon material possesses several advantages of high specific surface area, interconnected microporous structure, and N-doping which can provide abundant active sites, opened ionic channels, and improved wettability. Thanks to the multiple synergistic effect, the H-MPC-N-based electrode in 6 M KOH exhibits a high specific capacitance of 345 F g^{-1} at 0.5 A g^{-1}, excellent rate capability with 78.2% retention, and outstanding cycle performance. Furthermore, the flexible solid-state symmetric supercapacitor assembled with H-MPC-N and PVA/KOH gel electrolyte shows excellent flexibility and stability, and delivers a high energy density of 7.92 W h kg^{-1} at the power density of 250 W kg^{-1}. These promising results provide an effective valued-added window for the natural biomass or bio-waste to develop sustainable advanced carbon materials for the high-performance wearable and portable energy storage devices.

Acknowledgements

We are thankful to Analytical and Testing Center of Southwest Jiaotong University for supporting the SEM measurement. This work is supported by the National Natural Science Foundation of China (No. 51602265), the scientific and technological projects for International Cooperation of Sichuan Province (No. 2017HH0069), China Postdoctoral Science Foundation (2016M592692), and the Fundamental Research Funds for the Central Universities of China (A0920502051619-72) and the Independent Research Project of State Key Laboratory of Traction Power (Nos. 2017TPL_Z04, 2016TPL_Z03).

References

[1] J. Zhao, Y. Jiang, H. Fan, M. Liu, O. Zhuo, X. Wang, Q. Wu, L. Yang, Y. Ma, Z. Hu, Porous 3D Few-Layer Graphene-like Carbon for Ultrahigh-Power Supercapacitors with Well-Defined Structure-Performance Relationship, Adv. Mater. 29 (2017) 1604569.

[2] Y. Liu, Z. Xiao, Y. Liu, L.-Z. Fan, Biowaste-derived 3D honeycomb-like porous carbon with binary-heteroatom doping for high-performance flexible solid-state supercapacitors, J. Mater. Chem. A 6 (2018) 160-166.

[3] T. Lv, M. Liu, D. Zhu, L. Gan, T. Chen, Nanocarbon-Based Materials for Flexible All-Solid-State Supercapacitors, Adv. Mater. 30 (2018) 1705489.

[4] F. Beguin, V. Presser, A. Balducci, E. Frackowiak, Carbons and electrolytes for advanced supercapacitors, Adv. Mater. 26 (2014) 2219-2251.

[5] Y. Zhai, Y. Dou, D. Zhao, P.F. Fulvio, R.T. Mayes, S. Dai, Carbon Materials for Chemical Capacitive Energy Storage, Adv. Mater. 23 (2011) 4828-4850.

[6] Y. Zhang, X. Liu, S. Wang, L. Li, S. Dou, Bio-Nanotechnology in High-Performance Supercapacitors, Adv. Energy Mater. 7 (2017) 1700592.

[7] S. Dutta, A. Bhaumik, K.C.-W. Wu, Hierarchically Porous Carbon Derived from Polymers and Biomass: Effect of Interconnected Pores on Energy Applications, Energ Environ Sci 7 (2014) 3574-3592.

[8] C. Wang, D. Wu, H. Wang, Z. Gao, F. Xu, K. Jiang, Nitrogen-doped two-dimensional porous carbon sheets derived from clover biomass for high performance supercapacitors, J. Power Sources 363 (2017) 375-383.

[9] S. Song, F. Ma, G. Wu, D. Ma, W. Geng, J. Wan, Facile self-templating large scale

preparation of biomass-derived 3D hierarchical porous carbon for advanced supercapacitors, J. Mater. Chem. A 3 (2015) 18154-18162.

[10] X. Zhao, S. Wang, Q. Wu, Nitrogen and phosphorus dual-doped hierarchical porous carbon with excellent supercapacitance performance, Electrochim. Acta 247 (2017) 1140-1146.

[11] J. Chmiola, G. Yushin, Y. Gogotsi, C. Portet, P. Simon, P.L. Taberna, Anomalous Increase in Carbon Capacitance at Pore Sizes Less Than 1 Nanometer, Science 313 (2006) 1760-1763.

[12] A. Kajdos, A. Kvit, F. Jones, J. Jagiello, G. Yushin, Tailoring the Pore Alignment for Rapid Ion Transport in Microporous Carbons, J. Am. Chem. Soc. 132 (2010) 3252-3253.

[13] L. Wei, M. Sevilla, A.B. Fuertes, R. Mokaya, G. Yushin, Hydrothermal Carbonization of Abundant Renewable Natural Organic Chemicals for High-Performance Supercapacitor Electrodes, Adv. Energy Mater. 1 (2011) 356-361.

[14] Y. Zhu, S. Murali, M.D. Stoller, K.J. Ganesh, W. Cai, P.J. Ferreira, A. Pirkle, R.M. Wallace, K.A. Cychosz, M. Thommes, D. Su, E.A. Stach, R.S. Ruoff, Carbon-based Supercapacitors Produced by Activation of Graphene, Science 332 (2011) 1537-11541.

[15] M. Sevilla, J.A. Maciá-Agulló, A.B. Fuertes, Hydrothermal carbonization of biomass as a route for the sequestration of CO_2: Chemical and structural properties of the carbonized products, Biomass Bioenergy 35 (2011) 3152-3159.

[16] M. Sevilla, A.B. Fuertes, The production of carbon materials by hydrothermal carbonization of cellulose, Carbon 47 (2009) 2281-2289.

[17] C. Falco, N. Baccile, M.-M. Titirici, Morphological and structural differences between

glucose, cellulose and lignocellulosic biomass derived hydrothermal carbons, Green Chem. 13 (2011) 3273-3281.

[18] F. Liu, R. Yu, X. Ji, M. Guo, Hydrothermal carbonization of holocellulose into hydrochar: Structural, chemical characteristics, and combustion behavior, Bioresour. Technol. 263 (2018) 508-516.

[19] F.Y. Liu, M.H. Guo, Comparison of the characteristics of hydrothermal carbons derived from holocellulose and crude biomass, J. Mater. Sci. 50 (2015) 1624-1631.

[20] F. Liu, R. Yu, M. Guo, Hydrothermal carbonization of forestry residues: influence of reaction temperature on holocellulose-derived hydrochar properties, J. Mater. Sci. 52 (2016) 1736-1746.

[21] M. Sevilla, L. Yu, C.O. Ania, M.-M. Titirici, Supercapacitive Behavior of Two Glucose-Derived Microporous Carbons: Direct Pyrolysis versus Hydrothermal Carbonization, ChemElectroChem 1 (2014) 2138-2145.

[22] F. Gao, G. Shao, J. Qu, S. Lv, Y. Li, M. Wu, Tailoring of Porous and Nitrogen-rich Carbons Derived from Hydrochar for High-performance Supercapacitor Electrodes, Electrochim. Acta 155 (2015) 201-208.

[23] L. Zhao, L.Z. Fan, M.Q. Zhou, H. Guan, S. Qiao, M. Antonietti, M.M. Titirici, Nitrogen-containing hydrothermal carbons with superior performance in supercapacitors, Adv. Mater. 22 (2010) 5202-5206.

[24] C. Wang, D. Wu, H. Wang, Z. Gao, F. Xu, K. Jiang, Biomass derived nitrogen-doped hierarchical porous carbon sheets for supercapacitors with high performance, J. Colloid Interface Sci. 523 (2018) 133-143.

[25] A.B. Fuertes, M. Sevilla, High-surface area carbons from renewable sources with a bimodal micro-mesoporosity for high-performance ionic liquid-based supercapacitors, Carbon 94 (2015) 41-52.

[26] A.B. Fuertes, M. Sevilla, Superior capacitive performance of hydrochar-based porous carbons in aqueous electrolytes, ChemSusChem 8 (2015) 1049-1057.

[27] M. Sevilla, A.B. Fuertes, A Green Approach to High-Performance Supercapacitor Electrodes: The Chemical Activation of Hydrochar with Potassium Bicarbonate, ChemSusChem 9 (2016) 1-10.

[28] C. Falco, J.M. Sieben, N. Brun, M. Sevilla, T. van der Mauelen, E. Morallon, D. Cazorla-Amorós, M.M. Titirici, Hydrothermal carbons from hemicellulose-derived aqueous hydrolysis products as electrode materials for supercapacitors, ChemSusChem 6 (2013) 374-382.

[29] L. Peng, Y. Liang, H. Dong, H. Hu, X. Zhao, Y. Cai, Y. Xiao, Y. Liu, M. Zheng, Super-hierarchical porous carbons derived from mixed biomass wastes by a stepwise removal strategy for high-performance supercapacitors, J. Power Sources 377 (2018) 151-160.

[30] M. Sevilla, G.A. Ferrero, A.B. Fuertes, Beyond KOH activation for the synthesis of superactivated carbons from hydrochar, Carbon 114 (2017) 50-58.

[31] Y. Lv, F. Zhang, Y. Dou, Y. Zhai, J. Wang, H. Liu, Y. Xia, B. Tu, D. Zhao, A comprehensive study on KOH activation of ordered mesoporous carbons and their supercapacitor application, J. Mater. Chem. 22 (2012) 93-99.

[32] Z. Qiu, Y. Wang, X. Bi, T. Zhou, J. Zhou, J. Zhao, Z. Miao, W. Yi, P. Fu, S. Zhuo,

Biochar-based carbons with hierarchical micro-meso-macro porosity for high rate and long cycle life supercapacitors, J. Power Sources 376 (2018) 82-90.

[33] A.B. Fuertes, G.A. Ferrero, M. Sevilla, One-pot synthesis of microporous carbons highly enriched in nitrogen and their electrochemical performance, J. Mater. Chem. A 2 (2014) 14439-14448.

[34] Y. Li, G. Wang, T. Wei, Z. Fan, P. Yan, Nitrogen and Sulfur Co-doped Porous Carbon Nanosheets Derived from Willow Catkin for Supercapacitors, Nano Energy 19 (2016) 165-175.

[35] G. Ren, S. Li, Z.-X. Fan, J. Warzywoda, Z. Fan, Soybean-derived Hierarchical Porous Carbon with Large Sulfur Loading and Sulfur Content for High-performance Lithium–sulfur Batteries, J. Mater. Chem. A 4 (2016) 16507-16515.

[36] J. Zhou, J. Lian, L. Hou, J. Zhang, H. Gou, M. Xia, Y. Zhao, T.A. Strobel, L. Tao, F. Gao, Ultrahigh Volumetric Capacitance and Cyclic Stability of Fluorine and Nitrogen Co-doped Carbon Microspheres, Nat. Commun. 6 (2015) 1-8.

[37] J. Liu, W. Li, L. Duan, X. Li, L. Ji, Z. Geng, K. Huang, L. Lu, L. Zhou, Z. Liu, W. Chen, L. Liu, S. Feng, Y. Zhang, A Graphene-like Oxygenated Carbon Nitride Material for Improved Cycle-Life Lithium/Sulfur Batteries, Nano Lett. 15 (2015) 5137-5142.

[38] W. Yang, W. Yang, A. Song, L. Gao, L. Su, G. Shao, Supercapacitance of Nitrogen-sulfur-oxygen Co-doped 3D Hierarchical Porous Carbon in Aqueous and Organic Electrolyte, J. Power Sources 359 (2017) 556-567.

[39] J.Z. Chen, J.L. Xu, S. Zhou, N. Zhao, C.-P. Wong, Nitrogen-doped Hierarchically Porous Carbon Foam: A Free-standing Electrode and Mechanical Support for

High-performance Supercapacitors, Nano Energy 25 (2016) 193-202.

[40] J. Pang, W. Zhang, J. Zhang, G. Cao, M. Han, Y. Yang, Facile and sustainable synthesis of sodium lignosulfonate derived hierarchical porous carbons for supercapacitors with high volumetric energy densities, Green Chem. 19 (2017) 3916-3926.

[41] J. Pang, W.-F. Zhang, J.-L. Zhang, H.-M. Zhang, G.-P. Cao, M.-F. Han, Y.-S. Yang, Oxygen and Nitrogen Co-enriched Sustainable Porous Carbon Hollow Microspheres from Sodium Lignosulfonate for Supercapacitors with High Volumetric Energy Densities, ChemElectroChem 5 (2018) 1306-1320.

[42] J. Pang, W. Zhang, H. Zhang, J. Zhang, H. Zhang, G. Cao, M. Han, Y. Yang, Sustainable nitrogen-containing hierarchical porous carbon spheres derived from sodium lignosulfonate for high-performance supercapacitors, Carbon 132 (2018) 280-293.

[43] C. Zhong, Y. Deng, W. Hu, J. Qiao, L. Zhang, J. Zhang, A review of electrolyte materials and compositions for electrochemical supercapacitors, Chem. Soc. Rev. 44 (2015) 7484-7539.

[44] F. Zhang, Y. Lu, X. Yang, L. Zhang, T. Zhang, K. Leng, Y. Wu, Y. Huang, Y. Ma, Y. Chen, A Flexible and High-voltage Internal Tandem Supercapacitor Based on Graphene-based Porous Materials with Ultrahigh Energy Density, Small 10 (2014) 2285-2292.

[45] X. Wei, Y. Li, S. Gao, Biomass-derived interconnected carbon nanoring electrochemical capacitors with high performance in both strongly acidic and alkaline electrolytes, J. Mater. Chem. A 5 (2017) 181-188.

[46] L.J. Xie, G.H. Sun, F.Y. Su, X.Q. Guo, Q.Q. Kong, X.M. Li, X.H. Huang, L. Wan, W. song, K.X. Li, C.X. Lv, C.-M. Chen, Hierarchical Porous Carbon Microtubes Derived from Willow Catkins for Supercapacitor Applications, J. Mater. Chem. A 4 (2016) 1637-1646.

[47] Y. Huang, L. Peng, Y. Liu, G. Zhao, J.Y. Chen, G. Yu, Biobased Nano Porous Active Carbon Fibers for High-Performance Supercapacitors, ACS Appl. Mater. Interfaces 8 (2016) 15205-15215.

[48] Z. Hu, S. Li, P. Cheng, W. Yu, R. Li, X. Shao, W. Lin, D. Yuan, N,P-co-doped carbon nanowires prepared from bacterial cellulose for supercapacitor, J Mater. Sci. 51 (2015) 2627-2633.

[49] F. Gao, J.Y. Qu, Z.B. Zhao, Z.Y. Wang, J.S. Qiu, Nitrogen-doped Activated Carbon Derived from Prawn Shells for High-performance Supercapacitors, Electrochim. Acta 190 (2016) 1134-1141.

[50] M. Wahid, D. Puthusseri, D. Phase, S. Ogale, Enhanced Capacitance Retention in a Supercapacitor Made of Carbon from Sugarcane Bagasse by Hydrothermal Pretreatment, Energy Fuels 28 (2014) 4233-4240.

[51] Z. Lei, N. Christov, L.L. Zhang, X.S. Zhao, Mesoporous carbon nanospheres with an excellent electrocapacitive performance, J. Mater. Chem. 21 (2011) 2274-2281.

[52] X. Li, W. Xing, S. Zhuo, J. Zhou, F. Li, S.Z. Qiao, G.Q. Lu, Preparation of capacitor's electrode from sunflower seed shell, Bioresour. Technol. 102 (2011) 1118-1123.

Graphical Abstract